ACS Biomaterials SCIENCE & ENGINEERING

Article

Cite This: ACS Biomater. Sci. Eng. 2020, 6, 749−757

pubs.acs.org/journal/abseba

Acoustic Poration and Dynamic Healing of Mammalian Cell Membranes during Inkjet Printing

Srimanta Barui,[†,‡] Rachel E. Saunders,[†] Sharmistha Naskar,[‡] Bikramjit Basu,[‡] and Brian Derby*[,†]

[†]School of Materials, University of Manchester, Oxford Road, Manchester M13 9PL, United Kingdom

[‡]Laboratory for Biomaterials and Translational Center on Biomaterials for Orthopedic and Dental Applications, Materials Research Centre, Indian Institute of Science, Bangalore 560012, India

Supporting Information

ABSTRACT: We have investigated the effect of piezoelectric actuating voltage on cell behavior after drop on demand inkjet printing using mouse 3T3 cells as a model cell line. Cell viability after printing was assessed using a live/dead assay, Alamar Blue as an assay for cell proliferation, and propidium iodide (PI) and Texas Red labeled dextran molecular probes to assess cell membrane integrity. No significant difference was found for the cell death rate compared between an unprinted control population and after printing at 80, 90, and 100 V, respectively. However, cell proliferation was lower than that of the control population at all time points postprinting. Cell membrane integrity was quantified using PI and dextran probes of mean molecular weight of 3, 10, 40, and 70 kDa. Total membrane damage (assessed by PI) increased with increasing piezoelectric actuator driving voltage, and this was always greater than the unprinted control cells. The uptake of the labeled dextran only occurs after inkjet printing and was never observed with the control cells. The largest dextran molecular probe of 70 kDa was only taken up by cells after printing using the lower printing voltages of 80 and 90 V and was absent after printing at 100 V. At the two lower printing voltages, the membrane damage is recovered, and no dextran molecule penetrated the cells 2 h after printing. However, printing at 100 V leads to an increased uptake of 3 and 10 kDa dextran molecules, the retention of membrane porosity, and continued uptake of these 3 and 10 kDa dextran for greater than 2 h postprinting. We hypothesize that the change in membrane porosity with increasing actuation voltage can be explained by distinct nucleation and growth stages for pore formation in response to printing stress.

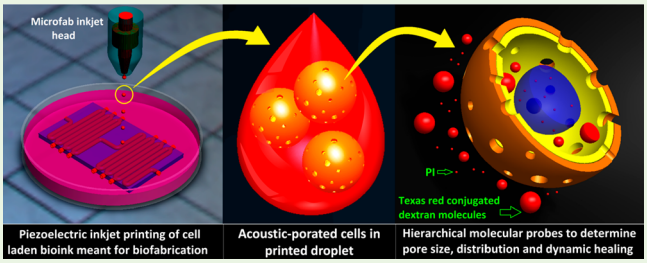

KEYWORDS: *piezoelectric-inkjet printing, cell printing, fibroblasts, cell viability, membrane permeability, molecular probes*

INTRODUCTION

During the past decade, the biomedical engineering community has explored the bioprinting of cells or cell laden biomaterials to manufacture high spatial resolution functional tissue constructs, using a range of printing methods based on nozzle microextrusion (direct writing), laser deposition (laser-induced forward transfer—LIFT), and inkjet printing.[1−7] More recently, a number of research groups have developed these high definition printing methods for the patterning and placement of cells and biological molecules (proteins, ECM, growth factors, etc.) for lab-on-a-chip or organ-on-a-chip applications.[8−10] However, the mechanical action and physical processes associated with these deposition techniques may lead to damage to cells or large molecules as has been quantified through earlier studies of printing or similar forces present in microfluidic devices.[11] It is thus apparent that microextrusion, inkjet printing (both thermal and piezoelectric), and laser based bioprinting can effectively deliver cells with "high throughput" and "precision", which are the prime precursors for more advanced functional lab-on-a-chip devices. Despite this, there has been little quantitative assessment of the effect of printing parameters on the cell damage and recovery, postprinting. This study attempts to quantify the relationship between printing parameters and cell damage during inkjet printing.

A number of different methods can be used to print or pattern surfaces with biological materials. Of these, nozzle based microextrusion is probably the most common technique used in bioprinting, because of its relative simplicity and the low cost of equipment. There is also a general belief that the low fluid shear rates, expected during nozzle extrusion, may result in a reduced level of cell damage during deposition. However, previous studies indicate that some damage to cells occurs using this methodology. Chang et al. investigated the postprinting viability of HepG2 cells using a proprietary extrusion based direct writing system and found that, after "long-term" postprinting culture conditions, viability was greater with larger nozzle diameters and driving pressure at the expense of proliferation.[12] Similar results were reported by Nair et al., who studied the effect of driving pressure and

Received: October 28, 2019
Accepted: December 2, 2019
Published: December 2, 2019

DOI: 10.1021/acsbiomaterials.9b01635
ACS Biomater. Sci. Eng. 2020, 6, 749−757

nozzle diameter on printed cell viability of murine endothelial cells; they also investigated the cell membrane properties postprinting and examined DNA degradation.[13] Cell apoptosis (<10%) was found to be triggered by a change in phosphatidylserine detected by Annexin-V and membrane permeability (necrosis), probed by both propidium iodide (PI) and Annexin-V. Their results showed a positive correlation of damage with increasing pressure and reducing nozzle diameter, which can be interpreted as indication of a sensitivity to fluid shear rate. Choi et al. carried out a study of cell damage induced by shear force using an extrusion based bioprinter to deposit C2C12 myoblasts.[14] Cell viability >90% was found 24 h after printing, and any change in viability was insignificant up to 14 days in culture. Blaeser used a microvalve based bioprinter to investigate the effect of shear force on the viability and stemness of human mesenchymal stem cells (hMSCs) postprinting and reported an inverse correlation between printing pressure and viability observed immediately after printing; interestingly, the stem cell phenotype remained unaltered.[15]

Laser based bioprinting methods, sometimes described as laser-induced forward transfer (LIFT), transfer material from a gel layer upon rapid adsorption of optical energy in a thin region of material immediately beneath the biomaterial to be transferred.[16] This method has the advantage of not requiring a liquid source material but may cause rapid accelerations and mechanical stresses during operation. Hopp used LIFT bioprinting to transfer rat Schwann and astroglial cells[17] and found that around 80−85% cell membranes were remained intact after transfer. Guillemot et al. explicitly reviewed the governing aspects of the physical parameters involved in laser bioprinting[18] and showed that surface tension, rheological characteristics, the initial film thickness of the bioink, and the laser pulse amplitude control the jetting process, while hydrodynamics associated with the impact conditions had a strong influence on cell viability and postprinting cell functionalities. Baron used human osteosarcoma cells with a Biological Laser Printing (BioLP) process and demonstrated the minimal expression of heat shock protein, indicating the absence of any significant printing-induced cell damage due to heat or shear stress.[19]

Inkjet printing has a number of advantages as a bioprinting process, including high spatial resolution and the ability to print multiple materials in the same process, as reviewed recently by Saunders and Derby.[20] However, it requires lower viscosity fluids and operates at significantly higher shear rates than nozzle microextrusion. Xu et al. studied the inkjet printing of Chinese hamster ovary (CHO) cells and rat neuronal cells using a thermal inkjet printer and reported a cell viability of 74% after printing neuronal cells, although the cells retained their phenotype and saw no further damage after 15 days in culture.[21] Saunders reported cell survival rates >90% after piezoelectric inkjet printing, using the human derived cell line HT1080, but in this case the cell survival rate decreased with increasing actuation voltage, which is believed to indicate a sensitivity to the fluid pressure or shear rate during printing.[22] Yamaguchi et al. reported similar cell survival rates to Saunders with around 90% of Sf9 cells surviving 1 h after piezoelectric inkjet printing.[23] Using a piezoelectric drop-on-demand (DOD) inkjet dispensing system, Park et al. demonstrated the efficacy of multipatterning of RGB fluorophore stained NIH3T3 and HEK293A cell laden bioinks in a coculture condition where they demonstrated an instant as-printed cell viability of 98.6%.[24] Cui et al. carried out a more sophisticated study of printing-induced membrane damage in Chinese hamster ovary (CHO) cells after thermal inkjet printing.[25] Texas red conjugated dextran molecules of different molecular weight were used as time dependent transmembrane permeability probes following procedures that had been successfully used previously to probe pore sizes in the cell membrane. They found transient permeability, through the formation of submicron membrane porosity after printing, but observed complete healing of membrane porosity 2 h after printing.

In this study we investigate the effect of piezoelectric inkjet printing on 3T3 mouse fibroblast cells. The 3T3 fibroblast cell line was selected as a model in this study because of its well-known resilience and ease of culture. Thus, it provides a potential upper bound limit to cell damage. Here, we investigate the effect of some piezoelectric inkjet printing parameters on 3T3 cell viability, proliferation, printing-induced cell membrane poration, and associated dynamic healing using Texas Red conjugated dextran molecular probes of a range of molecular weights.

RESULTS AND DISCUSSION

In this study, we have been able to produce a better understanding of the influence of printing parameters on cell membrane damage and damage recovery after piezoelectric inkjet printing. This shows that a major effect of the mechanical forces experienced during printing is the formation of pores in the cell membrane. The use of different sizes of molecular probes to characterize pore dimensions and lifetime postprinting gives a more complete picture of cell behavior than can be determined using simple cell death and cell metabolism assays.

Bioink Rheology and Printability Assessment. Cone−plate viscometry allows one to study the Newtonian or slightly shear thinning nature of the cell suspended bioink from the flow sweep data, where an almost constant static viscosity of ∼1.4 mPa s was recorded (Figure 1). On the other hand, dynamic viscosity was monitored with the variation in angular

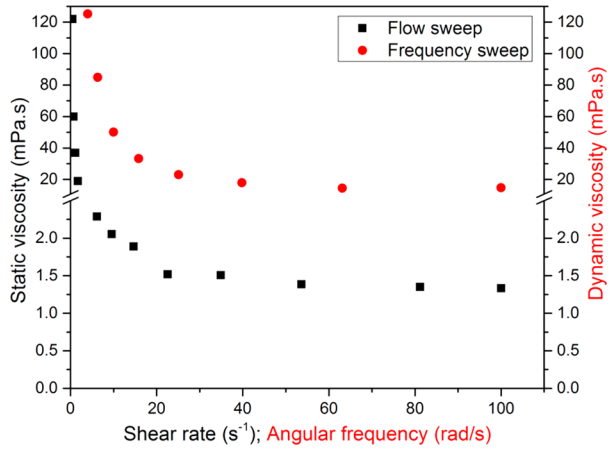

Figure 1. Fluid physics of ink governs the inkjet printability. Static and dynamic viscosities of the cell suspension were measured using a cone−plate viscometer. The almost constant static and dynamic viscosities at higher shear rate and angular frequency, respectively, implicate the Newtonian and laminar flow characteristics. The dynamic viscosity was well within the range to allow inkjet printability (≤30 mPa s).

DOI: 10.1021/acsbiomaterials.9b01635
ACS Biomater. Sci. Eng. 2020, 6, 749−757

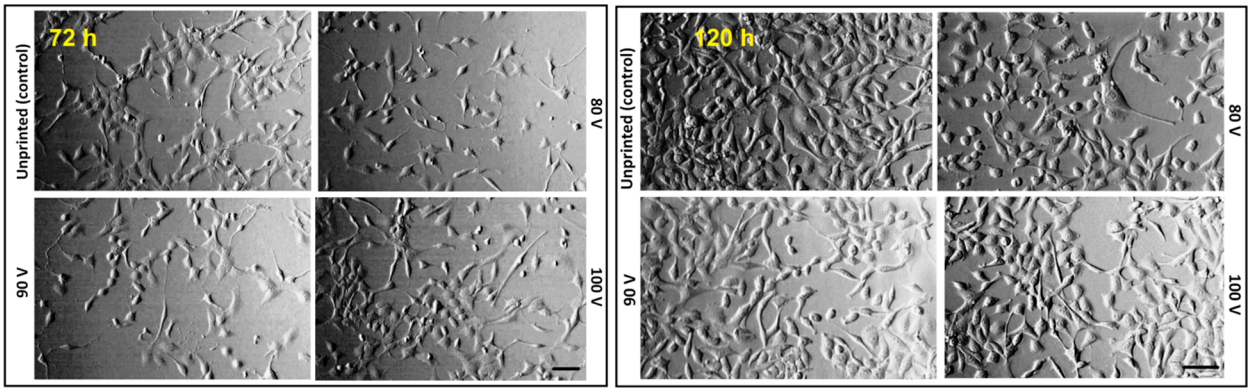

Figure 2. Optical DIC images of postprinted fibroblast cells reveal the morphological characteristics of the postprinted cells after 72 and 120 h of incubation. It was interesting to observe that, with increasing voltage, the number of printed cells increased. The cells printed with 100 V driving waveform exhibited enhanced spreading with time. Scale bar: 100 μm.

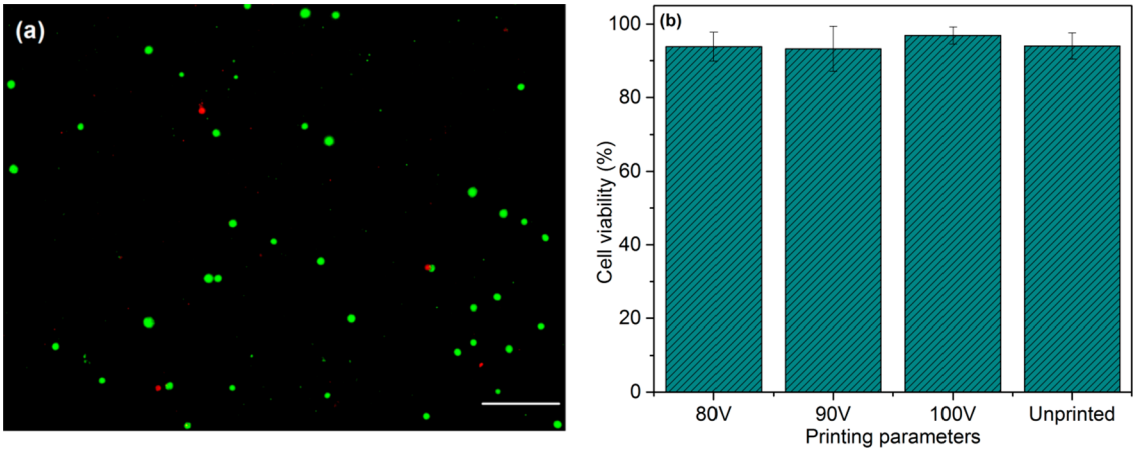

Figure 3. Live–dead assay of cells 2 h postprinting. (a) Fluorescent microscopy image of cells after printing at 80 V (green live, red dead). Scale bar: 100 μm. (b) Cell viability (% live cells) from n = 3 replicates (26 images each) at each printing condition and unprinted control, error bar = ±SD of data.

frequency. An almost constant dynamic viscosity of 14.6 mPa s, separately, was observed, both of which are well within the prescribed range for printability (≲30 mPa s).[6,26] The bioink interfacial tension was measured at 87.4 mN m^{-1}, which is a little higher than that of distilled water (72 mN m^{-1}).

These rheological measurements are necessary to calculate the appropriate characteristic dimensionless numbers for printability assessment,[6] which essentially depends on the fluid physical properties (density, viscosity, surface tension, flight velocity, etc.). The dimensionless constant Z (the inverse of the Ohnesorge number, Oh) has been used previously in the literature to define the inkjet printability of inks:

$$Z = \frac{(l\gamma\rho)^{1/2}}{\eta} = \frac{1}{Oh} \quad (1)$$

where η, γ, ρ, and l are the dynamic viscosity, surface tension, density, and the characteristic length associated with the droplet ejection which in most of the cases are considered as the orifice diameter. The condition for ink printability is defined by $1 < Z < 10$.[20,27] If $Z < 1$, viscous dissipation impedes drop formation, whereas when $Z > 10$ an extended ligament forms behind the ejected drop, which breaks into one or more small satellite drops, the presence of which reduces resolution and fidelity. Using our experimental values for viscosity and surface tension results for the 3T3 bioink suspension, we find $Z \sim 5$ ($Oh \sim 0.2$), indicating its printability.

Printed Cells Morphology under DIC Optical Microscope. Cell morphologies at 72 and 120 h postprinting are shown in Figure 2 for the three actuating voltages and a control unprinted sample. Under all conditions, the cells adhere and spread on the bottom of the well and grow toward confluence. After 120 h postprinting, the unprinted control shows greater cell multiplication which one can perceive even without any quantification. Similar behavior of cells after piezoelectric inkjet printing has been reported previously.[22] It can be clearly seen from the images that, with higher actuation voltage, a greater number of cells were deposited. We interpret this as indication a larger number of cells deposited at higher printing voltages because it is known that the drop volume becomes larger with increasing printing voltage,[20] and that a cell tends to spread more if its neighborhood is populated with a large number of similar cells.

Postprinting Cell Viability and Proliferation. A representative image of one of the printed samples (printed at 80 V) following the live/dead assay is presented in Figure 3a. The round cell shapes are anticipated as 2 h of incubation is not sufficient for extensive cytoskeletal spreading on a tissue culture plate. From the fluorescent image, it can be clearly seen that the majority of fibroblast cells have survived. Figure 3b

DOI: 10.1021/acsbiomaterials.9b01635
ACS Biomater. Sci. Eng. 2020, 6, 749–757

exhibits the survival statistics for cells printed at the three voltages compared with an unprinted control where the cell laden bioink was extruded pneumatically (minimum pressure to onset the dispensing) through the same nozzle without printing. In all cases, cell viability is >90%, with the cells printed at 100 V showing the highest viability at 97.0 ± 2.3%.

To better understand the statistical significances of the differences in the results, if any, an unpaired two-tailed t test was performed among all possible pairs of the groups. This showed no significant difference ($p > 0.05$) in cell viability between any possible pair comprising 80, 90, and 100 V and unprinted control samples. It is notable that this behavior is different from that reported by Saunders et al. for the printing of the human derived cell line HT1080, where a small but significant increase in cell death was reported as the printing voltage increased.[15] This confirms our hypothesis that the 3T3 cell line will show a robust response to cell dispensing stresses.

The Alamar Blue assay was performed by monitoring the printed cells benchmarked against the unprinted control samples up to 120 h in culture at 24 h intervals. The proliferation data were normalized with respect to the first time point (2 h) for each variant (different printing voltages and unprinted control). Figure 4 represents the proliferation data for all printing voltages and time points together with the unprinted control.

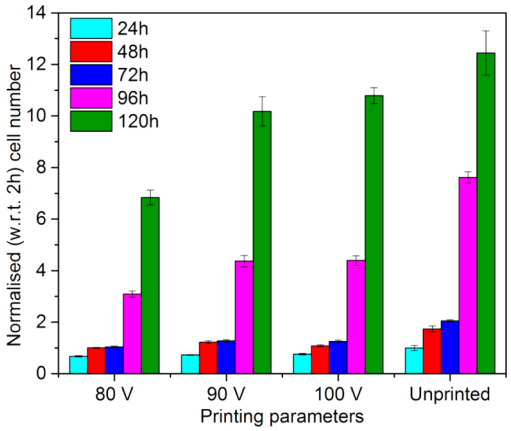

Figure 4. Viability and proliferation are the cell fate assays, which determine whether the bioprinting parameters induce compromised cytocompatibility. Postprinting cell proliferation after 24, 48, 72, 96, and 120 h, normalized (with respect to 2 h proliferation result). While the greatest proliferation was observed in the case of unprinted fibroblasts, when compared among the printing results, the cells printed using 100 V exhibited the best proliferation behavior.

In all cases, the normalized cell count increases with time in culture, and all printed samples show a slower proliferation rate when compared with the unprinted control at each time point. It is also clear that the cell proliferation rate increases with increasing printing voltage at all time intervals after printing. ANOVA was carried out to analyze the variation in cell viability between the three printing voltages and the control, the results of which are displayed in Table 1. It is clear that for all time intervals the probability of the null hypothesis (no significant difference among the mean values of groups of various printing conditions) to hold true is less than the value taken to indicate significance ($p < 0.05$).

To probe the origins of the statistical differences, a post-hoc Tukey HSD test (Table S1, see the Supporting Information) was performed. The proliferation data for the unprinted cells at each time point were found to be significantly higher in comparison with the cells printed using 80, 90, and 100 V ($0.05 < p$). This indicates that the printed cells were never able to attain the proliferation rate of the unprinted control at any given experimental time point for all three voltages. The Tukey test showed that 24 h after printing there was no significant difference in the proliferation rate for all three printing voltages, and at all time intervals there was no significant difference between the proliferation rates of the samples printed at 90 and 100 V. These observations and analyses suggest that, possibly counterintuitively, higher driving voltages induce overall less damage to cells during piezoelectric inkjet printing, leading to better postprinting proliferation behavior than observed with the lowest printing voltage. At lower actuation voltages, it was observed that drop ejection was less regular. We hypothesize that this may be the result of intermittent cell aggregation leading to temporary blockages of the nozzle orifice, which is less likely during the greater fluid flow amplitude at higher actuation voltages. These irregularities in drop ejection become more evident as the pulse amplitude is lowered further. It is thus possible that this drop formation irregularity may lead to increased stresses on some cells during drop ejection that do not occur at higher printing voltages. In order to confirm this hypothesis we would need to image fluid flow and cell migration within the nozzle immediately prior to drop ejection, a technically difficult experiment, even if the nozzle is transparent, which was beyond the technical scope of the printer set up used in this study.

The cell morphology and live/dead assay results (Figures 2 and 3) suggest that printing has very little effect on cell survival. Even when the Alamar Blue proliferation assay is used (Figure 4), the slightly lower proliferation rate seen after printing converges to that of the control with increasing printing voltage. The results of the present study therefore reveal significant differences from that reported by Saunders et al., who found a difference in cell proliferation at different printing voltages using the Alamar Blue assay. But they did not find the "systematic increase" in proliferation with printing voltage, as observed in the present study. It is not very straightforward to comment on the influence of printing conditions on cell behavior and population solely using the postprinting live/dead and proliferation assay which leads us to

Table 1. ANOVA for Timewise Interpretation of Cell Proliferation Using Different Printing Voltages (80, 90, 100 V)

proliferation time	F	critical F	nonsig./sig.	P value	critical P	inference
24 h	24.8	3.05	sig.	$p < 0.0001$	0.05	H_0 rejected
48 h	71.1	3.05	sig.	$p < 0.0001$	0.05	H_0 rejected
72 h	156.15	3.05	sig.	$p < 0.0001$	0.05	H_0 rejected
96 h	212.4	3.05	sig.	$p < 0.0001$	0.05	H_0 rejected
120 h	41.82	3.05	sig.	$p < 0.0001$	0.05	H_0 rejected

DOI: 10.1021/acsbiomaterials.9b01635
ACS Biomater. Sci. Eng. 2020, 6, 749−757

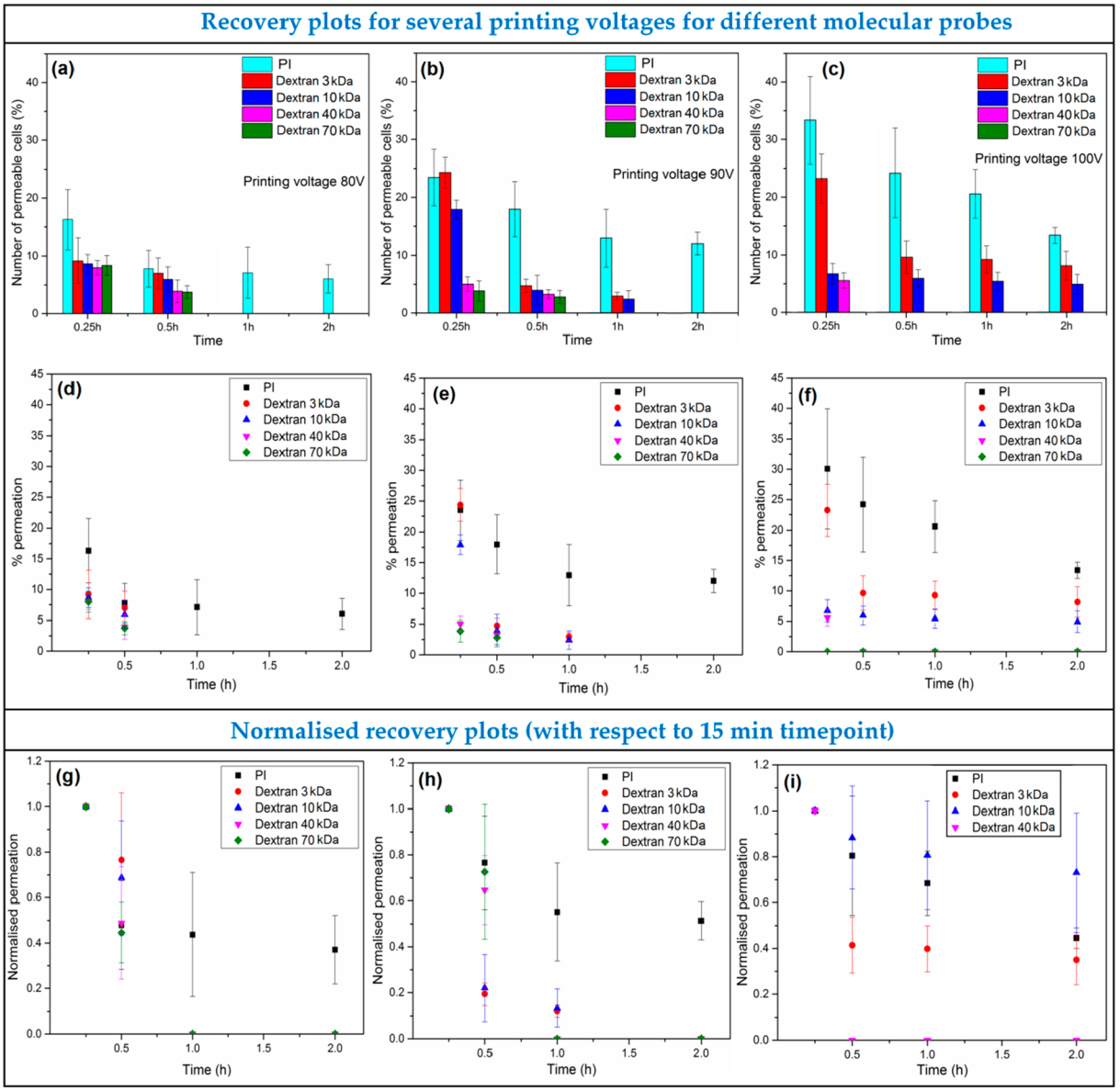

Figure 5. Transmembrane porosities are induced in the cells once they are exposed to physical stresses, leading to the development of membrane permeability. Very often, if not acute and severe, cells can repair the membranes over time. Membrane permeabilities of fluorophore tagged molecular probes with different molecular weights (PI, 3, 10, 40, and 70 kDa Texas red conjugated dextran molecules). Different postprinting time points (0.25−2 h) were chosen to observe the dynamic healing of membranes for (a, d) 80 V, (b, e) 90 V, and (c, f) 100 V. (g−i) Permeability of different probes normalized with the first time point (15 min) for each printing voltage (80, 90, and 100 V, respectively) to investigate the relative rate of healing.

interpret the cell membrane permeability and integrity studies to corroborate the results.

Cell Membrane Permeability. Cell membrane permeability after printing has been assessed using a hierarchical range of molecular probes with nominal diameters ranging from 1.68 to 12.0 nm. The data obtained using the cell permeability assays for time intervals of 15 min, 30 min, 1 h, and 2 h after printing are presented in Figure 5. Figure 5a−c shows the mean number of cells that were stained by each of the molecular probes after a given time interval to clearly indicate the different behavior of each probe. Figure 5d−f shows the data replotted to better identify the temporal change of probe penetration on a linear scale, and Figure 5g−i presents the probe concentration normalized by the concentration measured 15 min after printing to analyze the relative rate of dynamic healing.

In all cases the printed samples were compared with an unprinted control; however, only the smallest molecular probe, PI, was taken up by approximately 5% of the cells in the control population 15 min after dispensing. This decreases to about 1% of the unprinted cells 1 h after dispensing (pneumatically extruded, not printed) and is below the detection limit after 2 h (Figure 6). Hence, it is only possible to compare the printed cell behavior with the unprinted cells in the case of PI, the smallest molecular probe.

Comparing Figure 6 with Figure 5d−f, it is clear that at all three voltages a significantly greater number of the printed cells have absorbed PI than the unprinted sample, 15%, 20%, and 25% at 80, 90, and 100 V, respectively, compared with 5% for

DOI: 10.1021/acsbiomaterials.9b01635
ACS Biomater. Sci. Eng. 2020, 6, 749−757

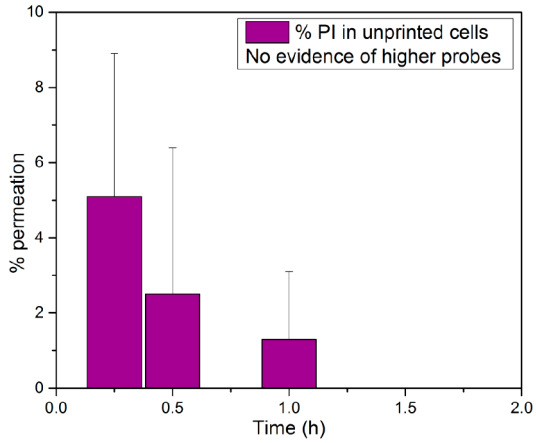

Figure 6. Permeability of propidium iodide (PI), the only probe having the equivalent stokes diameter of ~16 Å (smallest) into the unprinted 3T3 cells. It was found that the PI invasion is irregular due to rare pore formation in absence of printing, leading to the scattered nature of the data. The PI intrusion was found to be diminished after 2 h of pneumatic dispensing. This plot is provided separately as this cannot serve as control as there are both PI and dextran molecules invaded in printed cells.

the unprinted. The recovery of the unprinted cells is complete with no PI observable > 1 h after printing; however, for all three printing voltages there are a large number of cells that take up the PI even 2 h after printing. The data for the larger molecular weight probes showed similar behavior when comparing the results from cells printed at 80 and 90 V, but the results after printing at 100 V showed some differences. At the two lower printing voltages all 5 probes are present in the cells 15 min after printing and at a lower concentration after 30 min. After 1 h in culture postprinting none of the dextran probes are taken up by the cells printed at 80 V (Figure 5a), and this was also true for the 90 V samples after 2 h (Figure 5b). The 100 V printed cells (Figure 5c) did not show any presence of the 70 kDa dextran probe, and although there is significant take up of the 40 kDa probe 15 min after printing, this was not detected after 30 min. Conversely, unlike the samples printed with lower voltages, the dextran probes of 3 and 10 kDa continue to be detected in the printed cells after 2 h in culture.

In order to assess the behavior of the cells printed at 100 V to the low molecular weight dextran probes, further statistical analysis was carried out. ANOVA was carried out to determine whether there is any significant difference between the concentration of the 3 and 10 kDa probes at all time points after printing. As can be seen from Table 2 there is no significant difference among the data for the 10 kDa probe, but the null hypothesis is rejected for the 3 kDa probe. These data were further analyzed as a pairwise comparison using a post-hoc Tukey test, which is displayed in Table 3. This shows that there is no significant difference in the concentration of this probe between each pair of time points at 30 min, 1 h, and 2 h.

Our results show similarities with a prior study reported by Cui et al. for cell behavior after thermal inkjet printing.[25] They also used PI and labeled dextran probes to characterize cell permeability and pore formation using Chinese hamster ovary (CHO) cells.[25] In their study, it was found that PI penetrates printed cells up to 1.5 h after printing, but no PI was found 2 h after printing; however, no quantification of PI uptake was reported. This is in contrast with our results where PI

Table 2. ANOVA Table for Probewise (3 and 10 kDa Dextran) Interpretation of Membrane Permeability Printed Using 100 V in Different Postprinting Time (15 min, 30 min, 1 h, and 2 h)

	printing voltage: 100 V		
dextran probe	*F* statistics	$P_{\alpha=5\%}$	inference
3 kDa	*F*(3, 16): 26.56	1.8821×10^{-6} (significant)	H_0[a] rejected
10 kDa	*F*(3, 16): 0.37	0.77 (insignificant)	H_0 accepted

[a]H_0: null hypothesis—there is no significant difference in any permeability data of the 3 and 10 kDa probes printed using 100 V at different time points.

penetrates a large proportion of the cells even 2 h postprinting (Figure 5). The proportion of cells stained with PI increases with increasing printing voltage. It is worthwhile to note here that, with thermal inkjet printing, used by Cui et al., it is difficult to adjust the printing parameters to change the strain rate or stress experienced by the cells.

If we consider PI uptake as a generalized indicator of cell damage, as proposed by Malmgren,[28] this suggests that increasing the actuation pulse voltage increases the damage to cells during printing. This is commensurate with the observations of Saunders et al.,[22] who showed that the drop velocity increases with increased actuation voltage and observed a "small increase" in cell death as a result of increased stress on the cell during either drop generation or drop impact that occurs with the increased drop velocity as the actuation pulse amplitude increases. The insignificant dependence of the cell viability with printing voltage observed in this study may be due to the well-known stability and resilience of the murine 3T3 cell line and explain the difference in behavior compared to the HT1080 human fibrosarcoma cell line used by Saunders et al. Figure 5g–i shows the change in the proportion of cells that take up PI with time in culture, normalized by the result from 15 min after printing. We interpret the change in this parameter as indicating the rate of recovery (reduction in permeable area on membrane) of the cells after printing. Although the proportion of cells that are stained with PI increases with increasing voltage, the normalized recovery is approximately constant after 2 h for the lower printing voltages (80 and 90 V). This suggests that, given sufficient time, the membrane porosity generated during printing will fully heal after inkjet printing. For the highest printing voltage studied (100 V), the number of PI permeable pores is highest (Figure 5f) but despite the level of permeability continuously decreasing with time after printing, the 2 h time window is not sufficient enough to achieve the constant normalized recovery seen with printing at 80 and 90 V. It is not clear whether the reduced uptake of PI after thermal inkjet printing reported by Cui represents a universally lower cell stress compared with piezoelectric inkjet printing because only a single set of thermal printing conditions were studied.[25]

The uptake of dextran molecules after printing also shows a dependency on printing voltage, but a more complex behavior is seen than was the case with PI. We have taken the uptake of PI to be a generalized indication of cell membrane damage; the presence or absence of the labeled dextran of different molecular weight gives an indication of the size of the membrane pores. Thus, the behavior of the cells printed at 80

DOI: 10.1021/acsbiomaterials.9b01635
ACS Biomater. Sci. Eng. 2020, 6, 749–757

Table 3. Post-hoc Tukey HSD Test to Probe the Data Pairs (Postprinting Time), Responsible for the Statistically Significant Differences

probe, 3 kDa dextran; printing voltage, 100 V				
treatment pairs	critical Q (α = 0.05)	Q statistics	Tukey HSD p value	inference
15 min vs 30 min	4.04	9.8191	0.001	* p < 0.05 (sig)
15 min vs 1 h	4.04	10.0891	0.001	* p < 0.05 (sig)
15 min vs 2 h	4.04	10.8939	0.001	* p < 0.05 (sig)
30 min vs 1 h	4.04	0.2700	0.900	insignificant
30 min vs 2 h	4.04	1.0748	0.861	insignificant
1 h vs 2 h	4.04	0.8049	0.900	insignificant

Table 4. Dependence of Different Parameters Related to Printing and Printing-Induced Membrane Porosities with the Driving Voltage

Printing voltage	*Ease of droplet ejection and printing*	*Membrane pore number*	*Membrane pore diameter*	*Membrane healing time*
⇧	⇧	⇧	⇩	⇧
⇩	⇩	⇩	⇧	⇩

V (Figure 5a) can be interpreted as the formation of a population of membrane pores 15 min after printing that allow all 4 dextran probes to pass through the membrane of about 8% of the cells. The 70 kDa dextran probe has a diameter of approximately 12 nm; thus, the membrane porosity must be at least this size, accompanied by a further population of pores <3 nm in diameter that allow only the passage of PI. Printing at 90 V (Figure 5b) shows a smaller population of cells that allow passage of the 40 and 70 kDa dextran, but the number of cells permeable to the 3 and 10 kDa dextran after 15 min in culture has significantly increased compared to 80 V. Finally at 100 V (Figure 5c) none of the cells are permeable to the 70 kDa dextran even at the first time point (15 min) of culture postprinting, but the proportion of the 3 kDa dextran is similar to that printed at 90 V. Thus, although the total number of damaged cells (permeable to PI) increases with increasing voltage, the largest pore sizes are reduced. It should be noted that in Cui's study of thermal inkjet printing no cells were permeable to the 70 kDa probe after printing.[25]

With the cells printed at 80 and 90 V the recovery of the cell membrane reduces the mean size and number of the pores so that at 30 min the concentration of the larger dextran molecules decreases more rapidly, and after 2 h in culture the cells are fully recovered. The cell recovery after printing at 100 V shows different behavior with the membrane remaining permeable to 3 and 10 kDa dextran after 2 h in culture. On studying the recovery plot (Figure 5i) both of these probes show little change in concentration between 30 min and 2 h in culture, and any apparent change with time was shown to be not statistically significant (Table 3). Thus, although the higher printing voltage appears to reduce the maximum membrane pore size, it produces a larger population of smaller pores that remain open for significantly longer periods after printing than at the lower printing voltages.

However, the membrane permeability data reveal that as the printing voltage increases, the permeability of the membrane increases, and the damage remains present for longer times postprinting. Curiously, as the printing voltage increases, "smaller" pores are generated in "higher" numbers that could not be completely healed during the culture time of 2 h. To explain the anomalous behavior among cell viability and membrane porosity results at the highest printing voltage, we propose the following two hypotheses. In the first hypothesis, we explain the "reason" for the "higher number of smaller pores in higher printing voltage" and vice versa. If we consider pore formation to be a process of nucleation and growth driven by a reduction in the elastic energy of a ruptured membrane, thus, the increase in PI uptake with increasing printing voltage indicates a greater total number of pores; i.e., the pore nucleation rate is a function of the printing voltage. The growth of pore area will reduce the elastic energy in the strained membrane, and thus, we expect the growth rate to decrease with time. In the case of the cells printed at 100 V, we propose that the total pore area is such that pore growth is inhibited at a smaller mean pore area than occurs with the cells printed at the lower printing voltages (where fewer pores are nucleated). This explains the absence of the 70 kDa probes and increased permeability to the lower diameter dextran probes. In order to confirm this hypothesis it would be necessary to carry out further independent study of membrane poration, possibly through transmission electron microscopy (TEM) study of fixed cells prepared at each time point after printing. This was outside the scope of the present study and presents a clear avenue for future work. In the second hypothesis, we try to "correlate" the membrane permeability with the viability and proliferation results. For cell survival and proliferation, bigger membrane pores are deteriorative. As a result, the postprinting cell viability and proliferation rate might be lower in the case of printed cells using lower voltages, as the droplet ejection was not smooth (due to lower waveform amplitude and less ejection velocity) and stable as compared to those printed using higher voltage (100 V), during ejection. Therefore, we anticipate the win of small diameter membrane pores over the bigger one for better cell survival and functionality postprinting, even if the smaller pores are higher in number.

CONCLUSIONS

The general findings of this study are summarized in Table 4 with the two rows showing the trends in behavior at the highest and lowest printing voltages studied. It is generally easier to generate stable drops at a higher printing voltage, but this is accompanied by an increase in the total porosity of the cell membrane after printing, as characterized by the number

DOI: 10.1021/acsbiomaterials.9b01635
ACS Biomater. Sci. Eng. 2020, 6, 749−757

of cells permeable to PI. As expected, the time taken to recover from the printing-induced damage also increased with printing voltage. The maximum pore size in the damaged cell membrane appears to be reduced at the highest printing voltage, despite the total pore area increasing. We hypothesize that this indicates slightly different driving forces for pore nucleation and growth which needs a separate set of studies with extensive TEM imaging on fixed cells to directly count and measure the pore dimensions in individual cells at each time point after printed in individual driving voltages.

Finally, this study shows that although it is possible to use inkjet printing to deposit cells and that cell survival and proliferation are maintained for the vast majority of the printed cell population, there is significant short-term damage to the cell membrane that persists for hours after the printing operation. An interesting feature of our results is the observation that both the total area of pores and the maximum pore size are functions of the actuating pulse used to generate the drops. Thus, it may be possible to use inkjet delivery as a method to control the pore formation in cells, with potential applications in gene delivery and other cell modification procedures providing a useful tool for biotechnology. To assess and validate this potential will require significant further study.

■ ASSOCIATED CONTENT

Supporting Information

The Supporting Information is available free of charge at https://pubs.acs.org/doi/10.1021/acsbiomaterials.9b01635.

Experimental materials and bioink characterization, schematic illustration of the procedure adapted to prepare the 3T3 cell laden bioink, printing protocols and methodology, schematic of the inkjet printing set up employed to print 3T3 murine fibroblasts, postprinting cell viability and proliferation, probing printing-induced membrane porosity, and a post-hoc Tukey HSD test (PDF)

■ AUTHOR INFORMATION

Corresponding Author

*E-mail: brian.derby@manchester.ac.uk.

ORCID

Bikramjit Basu: 0000-0002-9154-5553

Brian Derby: 0000-0001-5753-0166

Notes

The authors declare no competing financial interest.

■ ACKNOWLEDGMENTS

The authors would like to thank Dr. Louise Carney and Mr. Andrew Wallwork, for their technical support. This work was supported by the Henry Royce Institute for Advanced Materials, funded through EPSRC grants EP/R00661X/1 and EP/P025021/1; some of the equipment used was funded through the EPSRC grant "Challenges in High Resolution Inkjet Printing" EP/L012022/1. S.B. acknowledges the Commonwealth Scholarship Commission, UK, for provision of a split-site Ph.D. Scholarship.

■ REFERENCES

(1) Murphy, S. V.; Atala, A. 3D bioprinting of tissues and organs. *Nat. Biotechnol.* **2014**, *32*, 773.

(2) Nakamura, M.; Iwanaga, S.; Henmi, C.; Arai, K.; Nishiyama, Y. Biomatrices and biomaterials for future developments of bioprinting and biofabrication. *Biofabrication* **2010**, *2* (1), 014110.

(3) Mironov, V.; Visconti, R. P.; Kasyanov, V.; Forgacs, G.; Drake, C. J.; Markwald, R. R. Organ printing: Tissue spheroids as building blocks. *Biomaterials* **2009**, *30* (12), 2164−2174.

(4) Guillemot, F.; Souquet, A.; Catros, S.; Guillotin, B.; Lopez, J.; Faucon, M.; Pippenger, B.; Bareille, R.; Rémy, M.; Bellance, S.; Chabassier, P.; Fricain, J. C.; Amédée, J. High-throughput laser printing of cells and biomaterials for tissue engineering. *Acta Biomater.* **2010**, *6* (7), 2494−2500.

(5) Hinton, T. J.; Jallerat, Q.; Palchesko, R. N.; Park, J. H.; Grodzicki, M. S.; Shue, H.-J.; Ramadan, M. H.; Hudson, A. R.; Feinberg, A. W. Three-dimensional printing of complex biological structures by freeform reversible embedding of suspended hydrogels. *Science Advances* **2015**, *1* (9), e1500758.

(6) Derby, B. Printing and Prototyping of Tissues and Scaffolds. *Science* **2012**, *338* (6109), 921.

(7) Yoon, S.; Park, J. A.; Lee, H.-R.; Yoon, W. H.; Hwang, D. S.; Jung, S. Inkjet−Spray Hybrid Printing for 3D Freeform Fabrication of Multilayered Hydrogel Structures. *Adv. Healthcare Mater.* **2018**, *7* (14), 1800050.

(8) Dou, R.; Saunders, R. E.; Mohamet, L.; Ward, C. M.; Derby, B. High throughput cryopreservation of cells by rapid freezing of sub-μl drops using inkjet printing − cryoprinting. *Lab Chip* **2015**, *15* (17), 3503−3513.

(9) Vespini, V.; Coppola, S.; Todino, M.; Paturzo, M.; Bianco, V.; Grilli, S.; Ferraro, P. Forward electrohydrodynamic inkjet printing of optical microlenses on microfluidic devices. *Lab Chip* **2016**, *16* (2), 326−333.

(10) Sun, Y.; Zhou, X.; Yu, Y. A novel picoliter droplet array for parallel real-time polymerase chain reaction based on double-inkjet printing. *Lab Chip* **2014**, *14* (18), 3603−3610.

(11) Bae, Y. B.; Jang, H. K.; Shin, T. H.; Phukan, G.; Tran, T. T.; Lee, G.; Hwang, W. R.; Kim, J. M. Microfluidic assessment of mechanical cell damage by extensional stress. *Lab Chip* **2016**, *16* (1), 96−103.

(12) Chang, R.; Nam, J.; Sun, W. Effects of Dispensing Pressure and Nozzle Diameter on Cell Survival from Solid Freeform Fabrication−Based Direct Cell Writing. *Tissue Eng., Part A* **2008**, *14* (1), 41−48.

(13) Nair, K.; Gandhi, M.; Khalil, S.; Yan, K. C.; Marcolongo, M.; Barbee, K.; Sun, W. Characterization of cell viability during bioprinting processes. *Biotechnol. J.* **2009**, *4* (8), 1168−1177.

(14) Choi, Y.-J.; Kim, T. G.; Jeong, J.; Yi, H.-G.; Park, J. W.; Hwang, W.; Cho, D.-W. 3D Cell Printing of Functional Skeletal Muscle Constructs Using Skeletal Muscle-Derived Bioink. *Adv. Healthcare Mater.* **2016**, *5* (20), 2636−2645.

(15) Blaeser, A.; Duarte Campos, D. F.; Puster, U.; Richtering, W.; Stevens, M. M.; Fischer, H. Controlling Shear Stress in 3D Bioprinting is a Key Factor to Balance Printing Resolution and Stem Cell Integrity. *Adv. Healthcare Mater.* **2016**, *5* (3), 326−333.

(16) Xiong, R.; Chai, W.; Huang, Y. Laser printing-enabled direct creation of cellular heterogeneity in lab-on-a-chip devices. *Lab Chip* **2019**, *19* (9), 1644−1656.

(17) Hopp, B.; Smausz, T.; Kresz, N.; Barna, N.; Bor, Z.; Kolozsvári, L.; Chrisey, D. B.; Szabó, A.; Nógrádi, A. Survival and Proliferative Ability of Various Living Cell Types after Laser-Induced Forward Transfer. *Tissue Eng.* **2005**, *11* (11−12), 1817−1823.

(18) Guillemot, F.; Souquet, A.; Catros, S.; Guillotin, B. Laser-assisted cell printing: principle, physical parameters versus cell fate and perspectives in tissue engineering. *Nanomedicine* **2010**, *5* (3), 507−515.

(19) Barron, J. A.; Krizman, D. B.; Ringeisen, B. R. Laser Printing of Single Cells: Statistical Analysis, Cell Viability, and Stress. *Ann. Biomed. Eng.* **2005**, *33* (2), 121−130.

(20) Saunders, R. E.; Derby, B. Inkjet printing biomaterials for tissue engineering: bioprinting. *Int. Mater. Rev.* **2014**, *59* (8), 430−448.

(21) Xu, T.; Jin, J.; Gregory, C.; Hickman, J. J.; Boland, T. Inkjet printing of viable mammalian cells. *Biomaterials* **2005**, *26* (1), 93−99.

DOI: 10.1021/acsbiomaterials.9b01635
ACS Biomater. Sci. Eng. 2020, 6, 749−757

(22) Saunders, R. E.; Gough, J. E.; Derby, B. Delivery of human fibroblast cells by piezoelectric drop-on-demand inkjet printing. *Biomaterials* **2008**, *29* (2), 193−203.
(23) Yamaguchi, S.; Ueno, A.; Akiyama, Y.; Morishima, K. Cell patterning through inkjet printing of one cell per droplet. *Biofabrication* **2012**, *4* (4), 045005.
(24) Park, J. A.; Yoon, S.; Kwon, J.; Now, H.; Kim, Y. K.; Kim, W.-J.; Yoo, J.-Y.; Jung, S. Freeform micropatterning of living cells into cell culture medium using direct inkjet printing. *Sci. Rep.* **2017**, *7* (1), 14610.
(25) Cui, X.; Dean, D.; Ruggeri, Z. M.; Boland, T. Cell damage evaluation of thermal inkjet printed Chinese hamster ovary cells. *Biotechnol. Bioeng.* **2010**, *106* (6), 963−969.
(26) Derby, B. Bioprinting: inkjet printing proteins and hybrid cell-containing materials and structures. *J. Mater. Chem.* **2008**, *18* (47), 5717−5721.
(27) Derby, B. Inkjet Printing of Functional and Structural Materials: Fluid Property Requirements, Feature Stability, and Resolution. *Annu. Rev. Mater. Res.* **2010**, *40* (1), 395−414.
(28) Malmgren, L. Assessing the quality of raw semen: A review. *Theriogenology* **1997**, *48* (4), 523−530.

DOI: 10.1021/acsbiomaterials.9b01635
ACS Biomater. Sci. Eng. 2020, 6, 749−757